Güdümen, H., Aksoy, C., Tıraşoğlu, E. (2024). Evaluation on K shell Fluorescence Parameters of Lead-Free Superconducting Alloys. *The Black Sea Journal of Sciences*, 14(4), 1917-1928.

*The Black Sea Journal of Sciences*, 14(4), 1917-1928, 2024. DOI: 10.31466/kfbd.1483591

KFBD

**Karadeniz Fen Bilimleri Dergisi**
The Black Sea Journal of Sciences
ISSN (Online): 2564-7377 https://dergipark.org.tr/tr/pub/kfbd

Araştırma Makalesi / Research Article

# Evaluation on K shell Fluorescence Parameters of Lead-Free Superconducting Alloys

Hüseyin GÜDÜMEN[1], Canan AKSOY[2]*, Engin TIRAŞOĞLU[3]

**Abstract**

The fluorescence parameters of the K-shell such as X-ray intensity ratios ($K_i/K_j$,) the production cross-sections ($\sigma_{Ki,}$) the fluorescence yields ($w_K$) of the superconducting solder alloys SnIn (20:80,35:65;45:55,65:30,75:25) wt%+Bi(6)wt% were investigated by using Ultra-Low Ge detector. The samples were irradiated by 59.5 keV γ-rays from an $^{241}$Am annular radioactive source. The obtained results were compared to theoretical values. The observed data showed that alloying effect and charge transfer between the elemental composition induce the deviations with the theoretical values.

**Keywords:** X-ray, Cross-Sections, Solder.

# Kurşunsuz Süperiletken Alaşımların K Kabuğu Floresans Parametrelerinin Değerlendirilmesi

**Öz**

Süperiletken lehim alaşımları SnIn (20:80, 35:65; 45:55, 65:30, 75:25) ağırlık%+Bi(%6 ağırlık)'nin K-kabuğu floresans parametreleri, X-ışını yoğunluk oranları ($K_i/K_j$), üretim tesir kesitleri ($\sigma_{Ki}$) ve floresans verimleri ($w_K$), Ultra-Düşük Ge dedektörü kullanılarak incelenmiştir. Numuneler, $^{241}$Am halka şeklinde radyoaktif bir kaynaktan gelen 59.5 keV γ-ışınları ile uyarılmıştır. Elde edilen sonuçlar teorik değerlerle karşılaştırılmıştır. Gözlenen veriler, alaşım etkisinin ve element bileşimi arasındaki yük transferinin teorik değerlerden sapmalara neden olduğunu göstermiştir.

**Anahtar Kelimeler:** X-ışını, Tesir Kesitleri, Lehim.

[1]National Defence University, Turkish Military Academy, Department of Basic Science, Ankara, Turkiye, hsyngdmn@gmail.com
[2]Karadeniz Technical University, Technology Faculty, Department of Department of Electronics and Communication Engineering, Trabzon, Türkiye, cananaksoy@ktu.edu.tr
[3]Karadeniz Technical University, Department of Physics, Trabzon, Turkiye, engint@ktu.edu.tr

*Sorumlu Yazar/Corresponding Author
**Geliş/Received:** 16.05.2024 **Kabul/Accepted:** 18.11.2024 **Yayın/Published:** 15.12.2024

## 1. Introduction

Some lead-based alloys have been used for superconducting applications such as superconducting power lines, high-field magnets for MRI machines, nuclear fusion reactors and particle accelerators. However, the solder technology has been moved away to prefer lead free solders due to harmful effect of lead on environmental and human health with the restriction of ROHS and WHEE directives [Directive 2002/96/EC, Directive 2002/96/EC ]. The researchers have focused on to discover novel lead-free solders. Tin based solders can be alternative to replace of lead solders since Tin has high ductility, low melting point and adequate superconducting properties [Mousavi et al., 2016]. SnIn and SnInBi solders can be new candidate for superconducting technology, although the critical current of the solders is lower than the lead-based solders.

Lead-based superconducting alloys are generally used in MRI magnets and large magnets. However, the toxic nature of lead harms the environment and human health. Therefore, recently, researchers have been trying to produce alternative lead-free solders as efficient as the lead included solders such as PbBi, PbSn in terms of physical, electrical and magnetic properties. The current studies (Aksoy et al.., 2023, Mousavi et al., 2016; Mousavi et al, 2016; Aksoy vd., 2016; Mousavi vd., 2016; Brittles et al., 2016) claimed that SnInBi alloys in different composition may be used to replacement for soldering in the superconducting and aerospace applications.

X-ray fluorescence (XRF) spectroscopy is one of the most effective spectroscopic technique in the field used to determine the physical and chemical structures of atoms and molecules. This method is suitable for fast and multi-element analysis without causing damage. In addition, it enables simultaneous measurement of elements with high detection sensitivity in a liquid or solid, even in very small quantities (Cengiz, 2011). The XRF gives accurate results with the parameters which have been used in atomic, molecular and radiation physics, material science, environmental science, agriculture, forensic science, dosimetric computations for health physics, cancer therapy, elemental analysis. The chemical environment of the alloys are also important for many disciplines. The concentration variety in the alloys induce to change the sample properties including fluorescence parameters which can be explained by the chemical effect such as charge transfer

In this study, XRF parameters of five different alloys consisting of a mixture of Sn, In and Bi in different proportions have been studied. As a result of X-ray excitation of the chemical properties of these elements in the alloy, the changes in cross section, fluorescence efficiency and intensity ratios were investigated.

## 2. Experimental Procedure

In this study, samples were excited by using a 50 mCi $^{241}$Am radioactive ring source emitting a 59.5 keV energy photon and the fluorescence cross section, fluorescence yields and X-ray intensity ratios of Sn, In and Bi mixed alloys were calculated. The pure Sn, In, Bi elements were weighted, cleaned in the ultrasonic cleaner, melted in the crucible, waited for 30 minutes up to 350 ºC and casted in the 13 mm radius disc shape mould. The composition was chosen as $Sn_{35}In_{65}Bi_6$, $Sn_{45}In_{55}Bi_6$, $Sn_{65}In_{30}Bi_6$, $Sn_{20}In_{80}Bi_6$, $Sn_{75}In_{25}Bi_6$.

The prepared samples for the measurement were measured with the Ultra-LEGe semiconductor detector. They were excited by photons with an energy of 59.5 keV emitted from a 50 mCi $^{241}$Am ring source. The schematic geometry set up of the detector is seen in Figure 1. The angles of the incident photons and the emitted X-rays with respect to the surface of samples, θ1 and θ2, were equal to 45° and 90°, respectively. The actual counting time for K X-ray counts were 10000 seconds. The obtained spectra were analysed using the Nucleus program (Genie 2000).

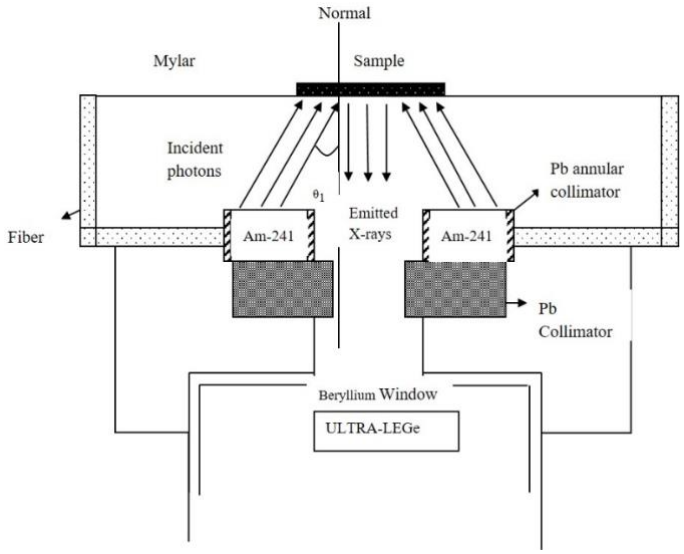


**Figure 1**: Geometry of Experimental set up of the Ultra-Low Germanium Detector.

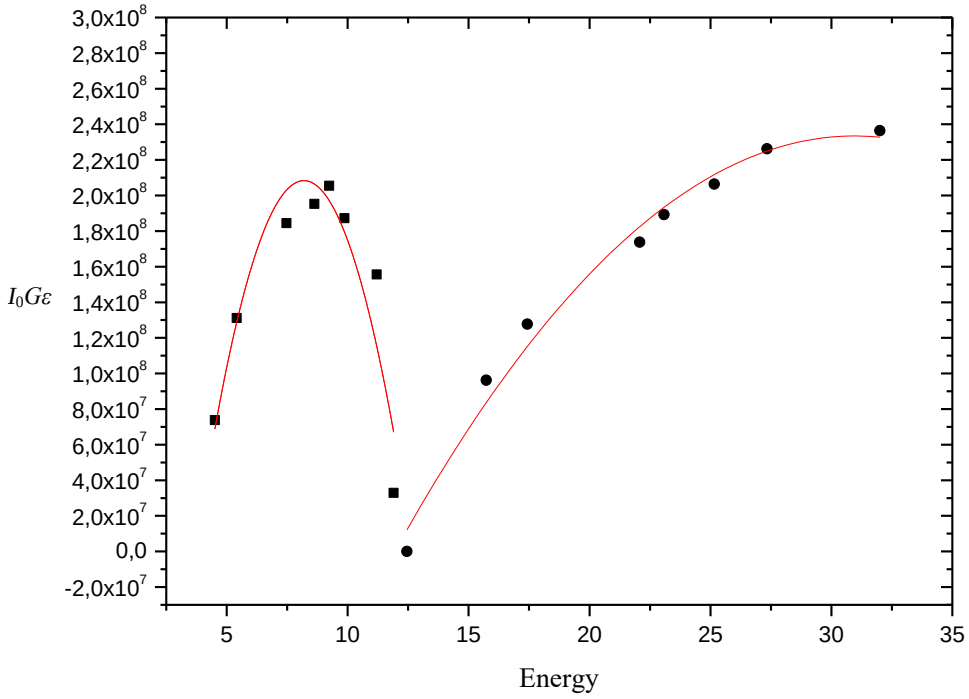


**Figure 2**. The factor $I_0G\varepsilon$ as a function of energy.

$I_0G\varepsilon$ yield curve were created for the experiment to calibrate the system as shown in Figure 2. In the efficiency for energies less than the Ge K absorption shore energy was calculated with the Equation (1).

$$Y = A + B_1.X + B_2.X^2 + B_3.X^3 \quad (1)$$

And the efficiency for energies greater than the Ge K absorption shore energy was calculated with the Equation (2).

$$Y = A + B_1.X + B_2.X^2 \quad (2)$$

Where the $A$, $B_1, B_2$ $and$ $B_3$are constant.

The characteristic X-rays generated by the excitation of the samples are absorbed by the atoms in the sample as they pass through the sample. Therefore, the X-ray intensity measured by the detector will differ from that emitted. In the studies based on intensity measurements, this difference disappears by dividing the measured X-ray intensity by the absorption correction factor. There is a relation between the emitted and measured X-ray intensity as following in Equation (3).

$$N_{measure} = N_{emit}\beta \quad (3)$$

Where β is the absorption factor and depends on the energy, sample atoms, incidence and exit angles of X-rays and sample thickness. Therefore, to find the characteristic X-rays emitted from the sample, the measured X-ray intensity β must be divided by the absorption factor. For this reason, β is called the absorption correction factor. It is given as in Equation (4):

$$\beta_{(i)} = \frac{1-\exp\left[-\left(\frac{(\mu/\rho)_{(\gamma)}}{\mathrm{Cos}\theta_1}+\frac{(\mu/\rho)_{(i)}}{\mathrm{Cos}\theta_2}\right)\rho D\right]}{\left(\frac{(\mu/\rho)_{(\gamma)}}{\mathrm{Cos}\theta_1}+\frac{(\mu/\rho)_{(i)}}{\mathrm{Cos}\theta_2}\right)\rho D} \quad (4)$$

In this Eq. 4, (μ/ρ) (γ) and (μ/ρ) (i) are the total mass reduction coefficients of the sample for the radiation from the source and the characteristic X-rays emitted, respectively. $\theta_1$ and $\theta_2$ are the mean angles of the radiation from the source and the characteristic X-rays emitted with the normal to the sample surface, respectively. According to the experimental geometry used in our study, the angle of incidence of $\theta_1$ 45° was kept constant, and the angle of X-rays coming out of the sample with the sample surface was 90°. If the amount of substance per unit area is $\rho_D$ (g/cm$^2$), it is found by dividing the weighted sample amount by the sample area. As shown in Equation (5):

$$\mu/\rho = \sum w_i (\mu/\rho)_i \quad (5)$$

In there, $w_i$ is weight percent of the element i$^{th}$, and $(\mu/\rho)_i$ is the mass reduction coefficient of the i$^{th}$ element at E energy.

The WinXCOM program was developed by Berger and Hubbel (Berger et al., 1998). It is used to calculate the total mass reduction coefficients at the respective energies of the elements.

### 2.1. The Fluorescence Parameters

The characteristic X-ray intensity is given as follows in Equation (6).

$$I = \frac{N}{\varepsilon.\beta} \quad (6)$$

Where, N, the area of corresponding X-ray peak, ε is detector efficiency of the characteristic X-ray and β self-absorption correction factor for the target material, which accounts for the absorption in the target of the incident photons and the emitted characteristic X-rays.

The experimental K-shell X-ray intensity ratios $I_{Ki}/I_{Kj}$ were evaluated using the Equation (7).

$$\frac{I_{Kj}}{I_{Ki}} = \frac{N_{Kj}}{N_{Ki}} \cdot \frac{\varepsilon_{Ki}}{\varepsilon_{Kj}} \cdot \frac{\beta_{Ki}}{\beta_{Kj}} \tag{7}$$

where $N_{Ki}/N_{Kj}$ (i,j=α, β) represents the ratio of the counting rates under the *Ki* and *Kj* peaks, $\beta_{Kj}/\beta_{Ki}$ is the ratio of self-absorption correction factors of the target that accounts for the absorption of incident photons and emitted K X-ray photons, and $I_0 G\varepsilon K_j / I_0 G\varepsilon K_i$ is the ratio of the detector efficiency values for $K_i$ and $K_j$ X-rays which is calculated from the fitted peak of the studied energy.

The following equations (8-10) are used to evaluate the fluorescence yield and fluorescence cross section data of the K shell,

$$\sigma_{Ki} = \sigma_K . \omega_K . f_{Ki} \qquad (i= \alpha, \beta) \tag{8}$$

$$\sigma_{Ki} = \frac{N_{Ki}}{I_0 G \varepsilon_{Ki} \beta_{Ki} t_i} \qquad (i= \alpha, \beta) \tag{9}$$

$$\omega_K = \frac{N_{Ki}}{I_0 G \varepsilon_{Ki} {\sigma_K}^P \beta_{Ki} t_i} = \frac{\sum \sigma_{Ki}}{{\sigma_K}^P} \qquad (i= \alpha, \beta) \tag{10}$$

$\sigma_K^P$, where $\sigma_K$ is the K-shell photo ionization cross-section of the given element for the excitation energy E (Scofield, 1973), $\omega_K$ is the K-shell fluorescence yield (Krause, 1979), and $f_{Ki}$ is the emission rate of the fractional X-ray for $K_i$ X-rays (Scofield, 1974), $t_i$ ($g.cm^{-1}$) is the sample thickness.

## 3. Results

Fgure 3. shows Kα and Kβ shell peaks for the pure Sn and In in the examined SnInBi alloys. The plot shows the X-ray intensity (counts) as a function of the channel number, which is proportional to the energy of the emitted X-rays. Distinct peaks corresponding to the Kα and Kβ transitions for both Sn and In are clearly visible, allowing for their identification and quantification within the alloy samples. This data likely serves as a reference for comparing and analyzing the X-ray spectra obtained from the actual SnInBi alloys to determine their fluorescence parameters.

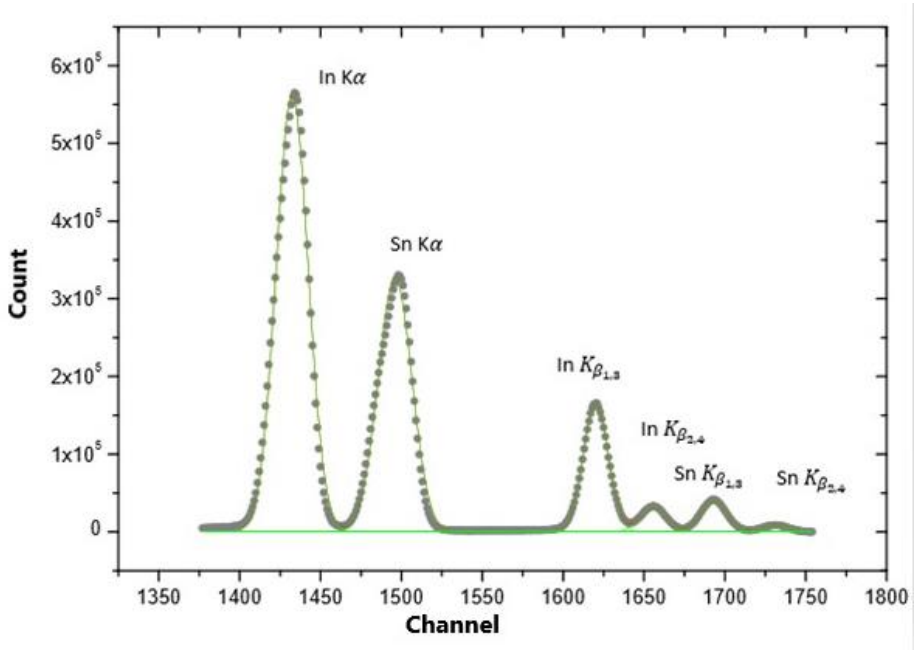


**Figure 3.** The K shell X-ray spectra of pure Sn and In elements

### 3.1. Fluorescence Cross-Section

K X-ray intensity ratios, fluorescence cross sections and fluorescence efficiency values for pure Sn, In and examined solders including Sn and In were experimentally measured by using an $^{241}$Am radioactive ring source that emits 59.5 keV photons.

K shell fluorescence cross sections for pure Sn, In and alloys are given in Table 1 in comparison with their theoretical values.

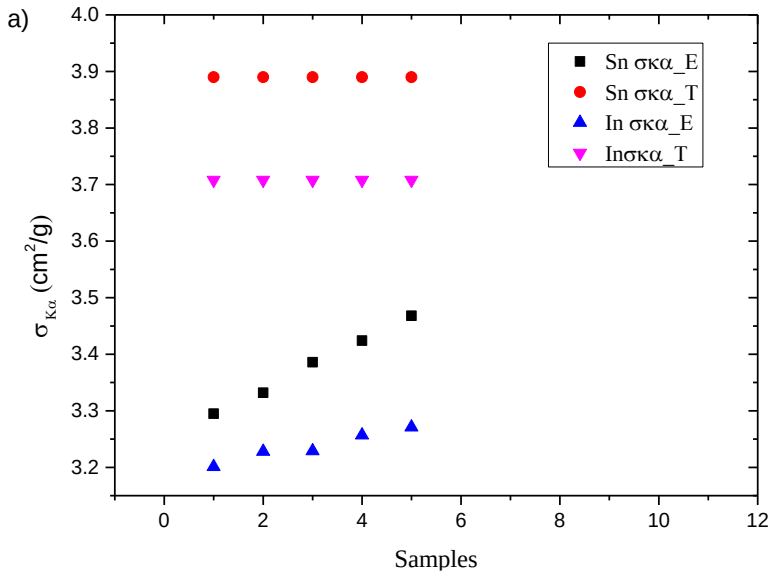

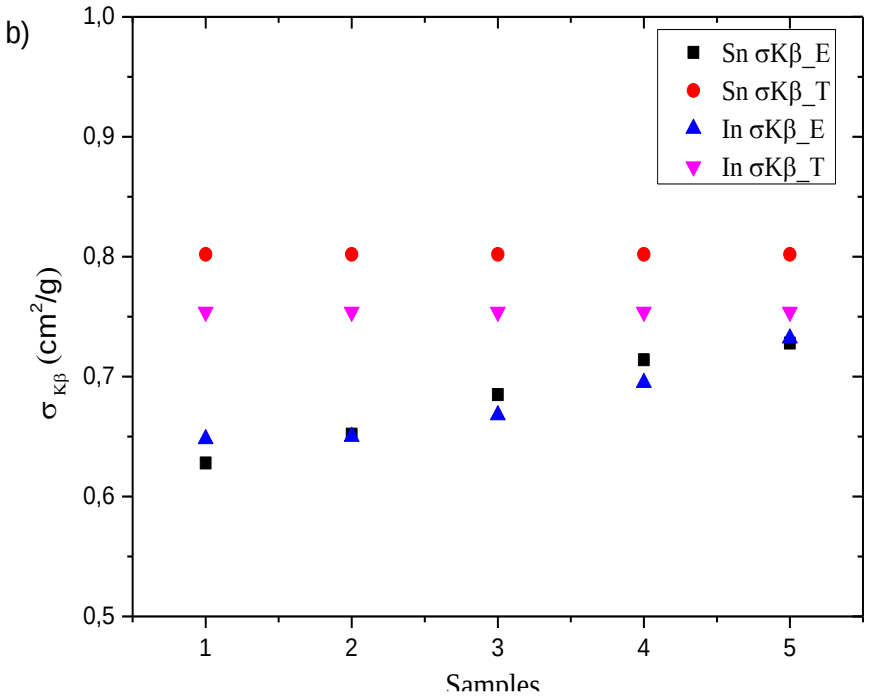


**Figure 4:** The plots show the comparison the of on the theoretical and experimental values of Sn and In the K-shell fluorescence cross- section a) $\sigma_{K\alpha}$ b) $\sigma_{K\beta}$ of the studied samples.

**Table 1.** The experimental and calculated $K_\alpha$ cross section values of the Sn and In in the studied alloys

| Samples | *Sn* $\sigma_{K\alpha}$ *Exp* ($cm^2/g$) | *Sn* $\sigma_{K\alpha}$ *Theo.*($cm^2/g$) | *In* $\sigma_{K\alpha}$ *Exp.* ($cm^2/g$) | *In* $\sigma_{K\alpha}$ *Theo.* ($cm^2/g$) |
|---|---|---|---|---|
| $Sn_{20}In_{80}Bi_6$ | 3.295±0.165 | 3.890 | 3.201±0.160 | 3.708 |
| $Sn_{35}In_{65}Bi_6$ | 3.332±0.167 | 3.890 | 3.228±0.161 | 3.708 |
| $Sn_{45}In_{55}Bi_6$ | 3.386±0.169 | 3.890 | 3.229±0.161 | 3.708 |
| $Sn_{65}In_{30}Bi_6$ | 3.424±0.171 | 3.890 | 3.257±0.162 | 3.708 |
| $Sn_{75}In_{25}Bi_6$ | 3.468±0.173 | 3.890 | 3.271±0.164 | 3.708 |

**Table 2.** The experimental and calculated $K_\beta$ cross section values of the Sn and In elements in the studied alloys

| Samples | Sn $\sigma_{K\beta}$ *Exp* ($cm^2/g$) | Sn $\sigma_{K\beta}$ *Theo.*($cm^2/g$) | In $\sigma_{K\beta}$ Exp ($gr/cm^2$) | In $\sigma_{K\beta}$ *Theo.*($cm^2/g$) |
|---|---|---|---|---|
| $Sn_{20}In_{80}Bi_6$ | 0.628±0.030 | 0.802 | 0.648±0.032 | 0.754 |
| $Sn_{35}In_{65}Bi_6$ | 0.652±0.032 | - | 0.650±0.032 | - |
| $Sn_{45}In_{55}Bi_6$ | 0.685±0.034 | - | 0.668±0.033 | - |
| $Sn_{65}In_{30}Bi_6$ | 0.714±0.035 | - | 0.695±0.034 | - |
| $Sn_{75}In_{25}Bi_6$ | 0.728±0.036 | - | 0.732±0.036 | - |

### 3.2. The Fluorescence Intensity Ratio

**Table 3**. The K shell intensity ratios $K_\beta/K_\alpha$ of Sn and In elements in the SnInBi alloys

| Samples | Sn $IK_\beta/IK_\alpha$ Exp | Sn $IK_\beta/IK_\alpha$ Theo. | In $IK_\beta/IK_\alpha$ Exp | In $IK_\beta/IK_\alpha$ Theo. |
|---|---|---|---|---|
| **1.** $Sn_{20}In_{80}Bi_6$ | 0.1906±0.009 | 0.2061 | 0.2025±0.010 | 0.2027 |
| **2.** $Sn_{35}In_{65}Bi_6$ | 0.1956±0.009 | - | 0.2013±0.010 | - |
| **3.** $Sn_{45}In_{55}Bi_6$ | 0.2024±0.010 | - | 0.2068±0.010 | - |
| **4.** $Sn_{65}In_{30}Bi_6$ | 0.2084±0.010 | - | 0.2133±0.011 | - |
| **5.** $Sn_{75}In_{25}Bi_6$ | 0.2098±0.010 | - | 0.2247±0.012 | |

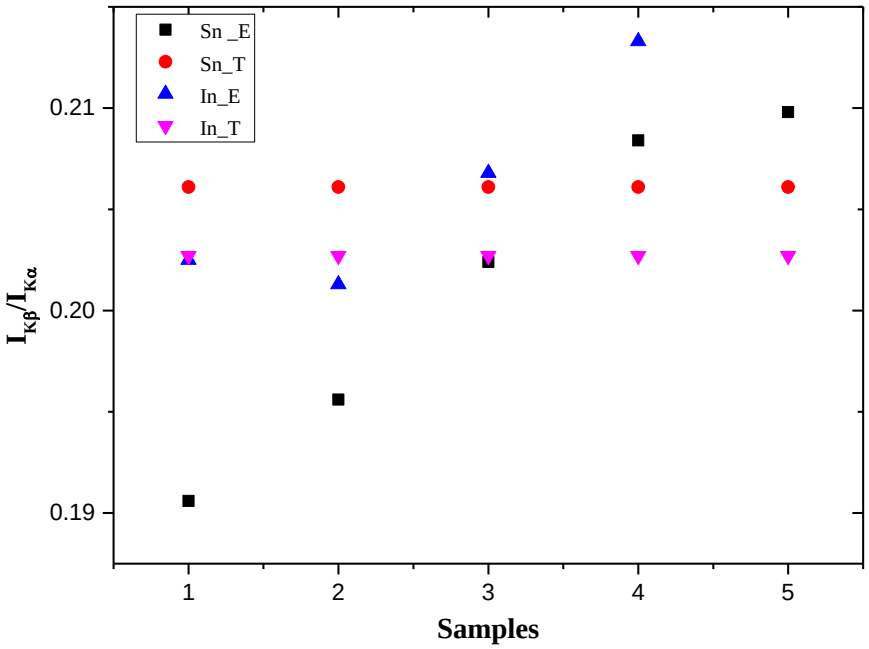


**Figure 5**. The comparison plot of the intensity ratio in terms of Sn and In elements in the SnInBi alloy samles.

**Table 4.** The K shell fluorescence efficiency of Sn and In alloys of the current study

| Samples | Sn $\omega_K$ | Sn $\omega_K^*$ | In $\omega_K$ | In $\omega_K^*$ |
|---|---|---|---|---|
| | Exp. | Theo. | Exp. | Theo. |
| $Sn_{20}In_{80}Bi_6$ | 0.719±0.036 | 0.860 | 0.734±0.037 | 0.851 |
| $Sn_{35}In_{65}Bi_6$ | 0.730±0.037 | - | 0.740±0.037 | - |
| $Sn_{45}In_{55}Bi_6$ | 0.746±0.037 | - | 0.743±0.037 | - |
| $Sn_{65}In_{30}Bi_6$ | 0.758±0.038 | - | 0.754±0.038 | - |
| $Sn_{75}In_{25}Bi_6$ | 0.769±0.038 | - | 0.744±0.037 | - |

## 4. Discussion

In the current study, the alloying effect of Sn and In elements in $Sn_xIn_yBi_6$ alloys on K shell fluorescence cross section and fluorescence yields, $K_\beta/K_\alpha$ X-ray intensity ratios were investigated. The experimental results obtained are given both tables and the plots with comparison with the theoretical values.

The obtained and theoretical data shows the difference for K shell X-ray fluorescence parameters. The main differences come from considered one is the transfer of valence electrons from one element in atoms to the other elements, and the second is the rearrangement of valence electrons with individual metal atoms (Aylıkcı, 2010).

It is known that X-ray emission spectra are affected by the chemical combination and physical properties of X-ray emitting atoms. Changes of X-ray fluorescence parameters for elements in chemical compounds or alloys are explained not only a result of changes in valence electronic configurations or the charge transfer effect, but also by changing in non-radiation transitions such as Auger, Coster-Kronig, or super Coster-Kronig, as radiative transitions are governed by non-radiation transitions. (Aylıkcı et al., 2010, Cengiz, et al. 2017, Güdümen,2017).

K-shell fluorescence parameters depend on the concentrations of the alloying elements. (Cengiz et al.,2014; Alım et al., 2018, Aylıkçı et al.,2010). The K shell cross sections of the studied samples were given in Table 1 and Table 2 that showed the differences of the theoretical and the experimental data of Sn and In element in the SnInBi alloys. According to the pure Sn element, in the Kα cross-sections decreasing were observed as 14.3% in the $Sn_{35}In_{65}Bi_6$ , 12.9% in the $Sn_{45}In_{55}Bi_6$, 11.9% in the $Sn_{65}In_{30}Bi_6$, 15.3% in the $Sn_{20}In_{80}Bi_6$ and 10.8 % in the $Sn_{75}In_{25}Bi_6$, respectively. It can be said that the increasing Sn content in the SnInBi alloys caused an enhancing in the Kα cross sections of both Sn and In as seen in the Table 1.

In the Table 2, The $K_\beta$ cross sections were given. According to the data, with the increasing Sn content in the SnInBi alloy, In terms of Sn element, the decrease was observed in the Kβ cross sections as 18.7% in the $Sn_{35}In_{65}Bi_6$ a, 14.6% in the $Sn_{45}In_{55}Bi_6$, 11.1% in the $Sn_{65}In_{30}Bi_6$, 21.7% in the $Sn_{20}In_{80}Bi_6$ alloy and 29% in the $Sn_{75}In_{25}Bi_6$ alloy.

As similar comparison with the $K_\alpha$ for In element in the SnInBi alloy, it was observed that increasing Sn content induce enhancement by increasing $K_\beta$ cross sections for In and Sn. The ratios of $K_\beta$ cross section 13.8% in $Sn_{35}In_{65}Bi_6$, 11,4 % in $Sn_{45}In_{55}Bi_6$, 7.8 % $Sn_{65}In_{30}Bi_6$, 14,1% in $Sn_{20}In_{80}Bi_6$, %16,2 in $Sn_{75}In_{25}Bi_6$. This situation can be explained by the population change in the valence state electrons by the rearrangement of the single atom with atoms between the valence energy levels. Besides, the plots in the Figure 4a and 4b show the comparison on the theoretical and experimental values of Sn and In the K-shell fluorescence cross- section of the studied samples that explains the phase changing cause the difference between the theoretical and experimental values.

In the current study, the intensity ratios were given in Table 3 and seen that there was not much difference between the alloys. It remained within the experimental error rate as 0-1 %. In the Figure 5 the comparison plot of the experimental and theoretical values of intensity ratios for Sn and In elements in the SnInBi alloys.

In table 4 and Figure 6, the K shell fluorescence yield $\boldsymbol{\omega_K}$ values of the studied alloys, comparison with theoretical pure Sn and experimental Sn values of fluorescence yield for each samples are as 15% in $Sn_{35}In_{65}Bi_6$, 13.2% in $Sn_{45}In_{55}Bi_6$, 16.3% in $Sn_{20}In_{80}Bi_6$, 11.8% in $Sn_{65}In_{30}Bi_6$, 12,5% in $Sn_{75}In_{25}Bi_6$ alloy samples.

The overall error in this study was estimated to be 6%. This error is the result of adding together the uncertainties in the different parameters used to evaluate sub-shell fluorescence yield and cross sections, namely target thickness (1%), peak area evaluation (1.5%), $I_0G\varepsilon$ product (2%), and the absorption correction factor (1.5%).

## 5. Conclusion

In this study, the fluorescence parameters of SnInBi alloys in different compositions were investigated. The obtained results were compared to the theoretical values. The results are in agreement with the theoretical values, and they showed that increasing Sn content in the SnInBi alloy enhances the fluorescence parameters. These findings may be useful for determining alloy compositions for various applications with solder systems. Specifically, the increase in fluorescence cross-sections, yields, and intensity ratios observed with increasing Sn content may affect the X-ray emission properties of the alloy and, consequently, its behaviour in applications. This data can provide important information for X-ray analysis of the alloy in soldering processes, for example, or for X-

ray characterization of the alloy in superconducting applications. In future work, the effect of varying Sn content in SnInBi alloys on fluorescence parameters could be investigated in more detail, and this data could be used to design new alloy compositions with better performance and suitability for various applications.

## References


Aksoy, C., Çakır, B., Koparan, E. T., Şimşek, C., Tıraşoğlu, E., Speller, S., Grovenor, C. R. M., Küçükömeroğlu, T., & Yanmaz, E. (2023). Lead-free superconducting alloys for superconducting applications. *Superconductor Science and Technology*, *36*(1), 015007. https://doi.org/10.1088/1361-6668/ac902f

Aksoy, C., Mousavi, T., Brittles, G., Grovenor, C. R. M., & Speller, S. C. (2016). Lead-free solders for superconducting applications. *IEEE Transactions on Applied Superconductivity*, *26*(3), https://doi.org/10.1109/TASC.2015.2511494

Alım, B., Han, I., & Demir, L. (2018). Alloying effect on K shell X-ray fluorescence cross-sections and yields in Ti-Ni based shape memory alloys. *Journal of Radiation Research and Applied Sciences*, *11*(2), 150-156. https://doi.org/10.1016/j.jrras.2017.09.003

Aylikci, N. K., Tiraşoğlu, E., Karahan, I. H., Aylikci, V., Cengiz, E., & Apaydin, G. (2010). Alloying effect on K shell X-ray fluorescence parameters and radiative Auger ratios of Co and Zn in ZnxCo1− x alloys. *Chemical Physics Letters*, *484*(4-6), 368-373. https://doi.org/10.1016/j.cplett.2010.01.016

Berger, M. J., & Hubbell, J. H. (1999). *XCOM: Photon cross-sections on a personal computer* (National Bureau of Standards Report NBSIR 87-3597). XCOM version 3.1.

Cengiz, E., Dogan, M., Biyiklioglu, Z., Cakir, D., Tirasoglu, E., & Apaydin, G. (2017). K X-ray fluorescence parameters of peripherally and non-peripherally tetra-substituted zinc (II) phthalocyanines. *Canadian Journal of Physics*, *95*(2), 125-129. https://doi.org/10.1139/cjp-2016-0378

Cengiz, E., Ozkendir, O. M., Kaya, M., Tirasoglu, E., Karahan, I. H., Kimura, S., & Hajiri, T. (2014). Alloying effect on K-shell fluorescence parameters of porous NiTi shape memory alloys. *Journal of Electron Spectroscopy and Related Phenomena*, *192*, 55-60. https://doi.org/10.1016/j.elspec.2013.11.003

Directive 2002/95/EC on the restriction of the use of certain hazardous substances in electrical and electronic equipment. (2003, January 27). *Official Journal of the European Union*, *L 37*, 19.

Directive 2002/96/EC on waste electrical and electronic equipment. (2003, January 27). *Official Journal of the European Union*, *L 37*, 24.

Dogan, M., Tirasoglu, E., Karahan, I. H., Aylikci, N. K., Aylikci, V., Kahoul, A., Cetinkara, H. A., & Serifoglu, O. (2013). Alloying effect on K X-ray intensity ratio and production cross section values of Zn and Cr in Zn Cr alloys. *Radiation Physics and Chemistry*, *87*, 130-134. https://doi.org/10.1016/j.radphyschem.2013.03.013

Güdümen, H. (2017). *Sn ve In elementlerinin oluşturduğu alaşımların X-ışını flouresans parametreleri üzerine alaşım etkisi* (Doctoral dissertation, Karadeniz Teknik Üniversitesi/Fen Bilimleri Enstitüsü/Fizik Anabilim Dalı).

Krause, M. O. (1979). Atomic radiative and radiotionless yields for K and L shells. *Journal of Physical and Chemical Reference Data*, *8*, 307-327. https://doi.org/10.1063/1.555581

Mousavi, T., Aksoy, C., Grovenor, C., & Speller, S. (2016). Phase evolution of superconducting Sn–In–Bi solder alloys. *IEEE Transactions on Applied Superconductivity*, *26*(3), 1-4. https://doi.org/10.1109/TASC.2015.2511497

Mousavi, T., Aksoy, C., Grovenor, C. R. M., & Speller, S. C. (2015). Microstructure and superconducting properties of Sn–In and Sn–In–Bi alloys as Pb-free superconducting solders. *Superconductor Science and Technology*, *29*(1), 015012. https://doi.org/10.1088/0953-2048/29/1/015012

Scofield, J. H. (1973). *Theoretical photoionization cross sections from 1 to 1500 kev*. *Lawrence Livermore Laboratory (UCRL)*, *51326*.

Scofield, J. H. (1974). Hartree-Slater calculations of electron binding energies and x-ray energies in neutral atoms. *Physical Review A*, *9*, 1041-1053. https://doi.org/10.1103/PhysRevA.9.1041